ACS APPLIED MATERIALS & INTERFACES

Research Article

Cite This: ACS Appl. Mater. Interfaces 2019, 11, 36444−36448

www.acsami.org

Multitag-Regulated Cascade Reaction: A Generalizable Ultrasensitive MicroRNA Biosensing Approach for Cancer Prognosis

Ruoyu Wang, Xiyu Zhu, Yunpeng Xing, Abdul Ghaffar Memon, Hanchang Shi, and Xiaohong Zhou*

State Key Joint Laboratory of ESPC, Center for Sensor Technology of Environment and Health School of Environment, Tsinghua University, Beijing 100084, China

Supporting Information

ABSTRACT: Ultrasensitive PCR-free microRNA (miR) analysis based on biosensors with enzyme-free nucleic acid amplification and reusable surface has great clinical significance in cancer prognosis. However, building such a biosensing strategy has long been challenging due to uncontrollable miR-triggered cascade amplifiers and insufficient sensing surface regeneration capability. To meet the challenge, for the first time, a general approach, named enzyme-free multitag-regulated cascade reaction (MCR), is developed to fabricate reliable trace miR biosensors. As a proof of concept, miR *let-7a* is detected on an evanescent wave fluorescent optical-fiber biosensing platform. The size and morphology of well-formed MCR assemblies (~1 μm in length) are characterized by atomic force microscopy. This MCR method achieves a 30 000-fold improved sensitivity (detection limit 0.8 fM) compared to the MCR-free system and can detect abnormal urinary miR levels in lung cancer patients. Moreover, the biosensor is robust enough to be reused for over 100 cycles, which greatly reduces the cost of single detection. In sum, MCR is developed as a generalizable ultrasensitive miR biosensing approach for cancer prognosis, which opens a broad field for facile enzyme-free biosensing applications by nucleic acid assembling regulation.

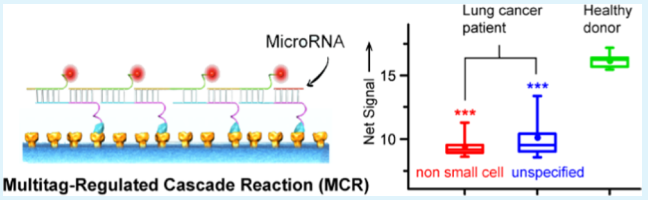

KEYWORDS: *biosensors, cancer prognosis, multitag-regulated cascade reaction, microRNA, signal amplification*

INTRODUCTION

Early diagnosis and treatment of cancer, as well as understanding the relationship between cancer markers and pathogenesis have been of practical and essential interest to scientists, doctors, and general public for a long time.[1,2] MicroRNAs (miRs) are noncoding RNAs (18−22 nt) that work as either tumor suppressors or oncogenic RNAs with abnormal expression level in cancerous cells, thus holding vast potential as cancer biomarkers.[3−5] To date, over 30% important human genome has been estimated to be the target of over 4000 identified miRs.[6,7] Low intracellular miR expression level calls for ultrasensitive analysis techniques, which are of great clinical significance in cancer prognosis. Currently, PCR-based assays are widely used,[8] which feature highly standardized sensitive analysis, but often at the expense of simplicity, facile operation, rapid analysis, or inexpensive instrumentation.[7,9] The development of reliable integrated PCR-free miR biosensors for clinic/household applications remains challenging. In principle, biosensors respond to specific recognition events at the functionalized solid−liquid interface.[10] However, due to their small sizes and low contents of body fluids, direct miR detection suffers from limited sensitivity,[4] thereby amplification is urgently needed. For example, nanomaterial-amplified ultrasensitive detection of miR based on electrochemical platforms have been reported.[11,12] Besides nanomaterial-amplified strategies, based on toehold-mediated strand displacement (TSD) mechanism,[13] nucleic acid cascades or assemblies represent another class of facile isothermal enzyme-free amplification strategies with superior features in cost, modularity, programmability, and universality.[14,15] For instance, hybridization chain reaction is a well-known cascade reaction during which an initiator (In) triggers the formation of long nicked duplex assemblies,[16] where miR could readily serve as the initiator (In). Although a homogeneous miR-triggered cascade assay has emerged in recent years, the development of miR biosensors based on solid−liquid interface, which usually can achieve higher sensitivity and simpler facility, has made much less progress.[17−20]

The major challenge in developing TSD amplification-based miR biosensors is that most biosensors rely on specific biorecognition signals at the transducer surface as a quantification basis and thus are sensitive to signaling distance, such as the evanescent wave optical biosensors and most electrochemical biosensors.[21−23] For example, a home-made optical-fiber evanescent wave fluorescence (FL) biosensor (Figure 1A), one of the earliest trials for reusable nucleic acid biosensing,[24,25] collects the FL excited within an exponentially decaying evanescent field around the optical fiber; therefore, the signals are greatly affected by the locations of fluorophores.[26] However, the binding of cascade assemblies to transducer frequently relies on monotag-regulated strategies

Received: August 13, 2019
Accepted: September 17, 2019
Published: September 17, 2019

DOI: 10.1021/acsami.9b14452
ACS Appl. Mater. Interfaces 2019, 11, 36444−36448

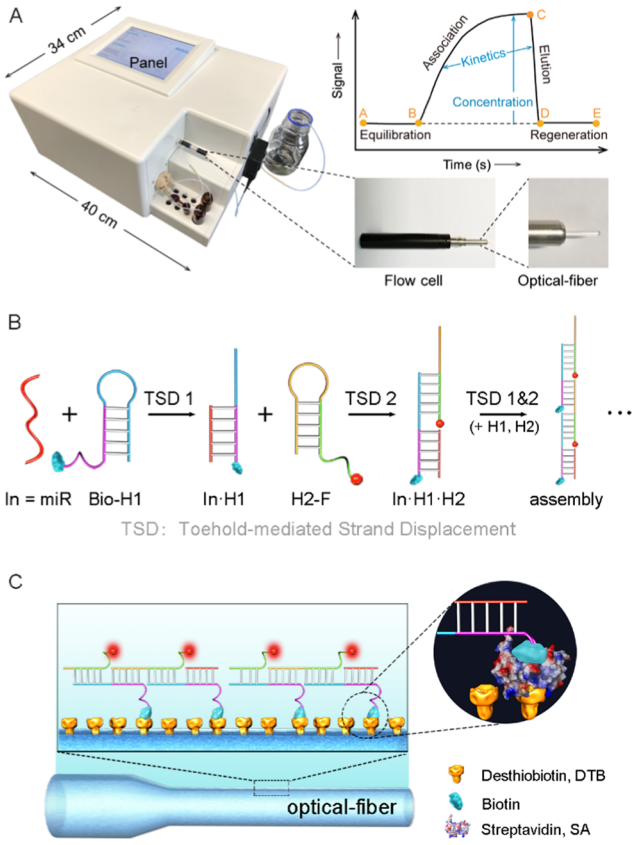

Figure 1. (A) Photograph of the developed optical-fiber biosensor. Inset: a representative sensorgram. Scheme of (B) miR-triggered cascade reaction and (C) multitag regulation on signaling-distance-sensitive optical-fiber biosensor.

such as sticky-end hybridization,[27] adsorption,[28] or other affinitive interaction,[29] leaving assemblies with broad size distribution[30,31] overhanging in bulk solution. The varying spatial distribution of fluorophores labeled on assemblies makes signaling-distance-sensitive biosensors prone to low sensitivity and even nonmonotonic responses.[19]

To meet the challenge, we first report a multitag-regulated cascade reaction (MCR) as a general miR amplification biosensing approach. Multisite biotinylated MCR products are designed to accommodate themselves onto the streptavidin (SA)-functionalized transducer to provide an approximately unified signaling distance for labeled fluorophores. The superior sensing performances of MCR approach are demonstrated on the optical-fiber platform: a limit of detection (LOD) down to 0.8 fM toward model miR (*let-7a*) and a clear discernment of urinary *let-7a* levels between lung cancer patients and healthy donors are achieved.

EXPERIMENTAL SECTION

See the Supporting Information for (1) materials and instruments, (2) optical-fiber-based fluorescent biosensor, (3) verification of TSD1 and TSD2 processes, (4) characterization of MCR assemblies by atomic force microscopy (AFM) measurements and gel electrophoresis, (5) preparation of DTB-functionalized optical-fiber sensing surface, (6) detection of miR in buffer/human urine using the optical-fiber-based biosensor, and (7) logistic fitting of the calibration curve (Tables S1–S3 and Figures S1–S9).

RESULTS AND DISCUSSION

Briefly, MCR is composed of a miR-triggered cascade and a followed surface regulation: first, the miR serves as an initiator (In) to trigger successive TSD of hairpins (Bio-H1 and H2-F) to form multiple linear duplex In·$(H1{\cdot}H2)_n$ assemblies as MCR products (Figure 1B). In the absence of miR, spontaneous hybridization of two hairpins is minor due to locked complementary domains. Robust cascade pathways can be achieved based on practical design guidelines[32] and computational tools.[33] To reduce the cost of single detection, desthiobiotin (DTB) molecules with moderate binding affinity toward SA[34,35] are used to prepare a reusable optical-fiber surface. Biotinylated MCR assemblies are designed to be anchored onto DTB-functionalized fiber surface using SA "glue", providing approximately unified signaling distances for labeled fluorophores (Figure 1C). After evanescent wave excitation, the signals generated by these fluorophore-labeled MCR assemblies can be analyzed based on the optical-fiber platform. Moreover, SA-MCR complexes can be effectively washed off to regenerate the DTB surface. As a control, monotag-regulated cascade reaction is conducted using biotinylated In (Bio-In) (Figure S1A).

To demonstrate the implementation of miR-triggered cascade reaction, a dual-labeled H1 beacon system is applied to validate TSD1 (Figure 2A). After annealing, the formation

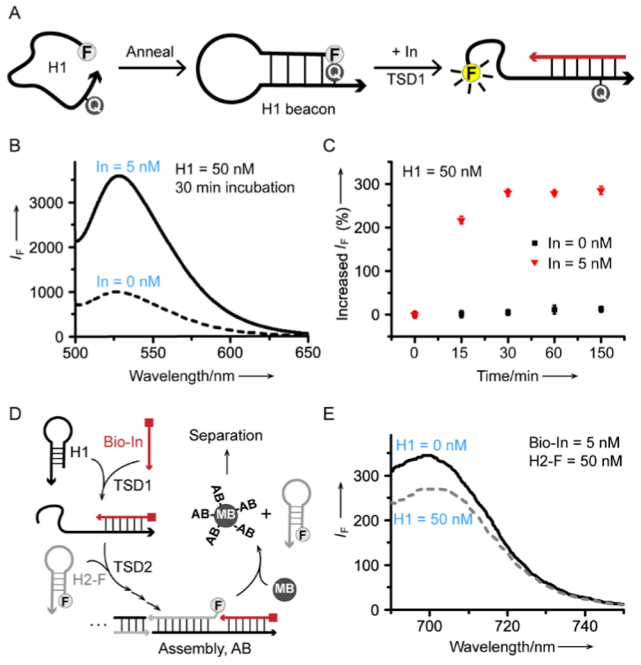

Figure 2. (A) Scheme of TSD1. (B) FL spectra and (C) increased I_F against time of H1 beacon-based system. (D) Scheme of TSD2. (E) FL spectra of supernatant. I_F = FL intensity.

of H1 hairpin places fluorophore (F) in close proximity to its quencher (Q), resulting in a low FL background; after TSD1, the formation of In·H1 separates F from Q, leading to an obvious FL recovery. As shown in Figure 2B,C, over 250% I_F increase in FL peak could be observed 30 min after the addition of In. Next, TSD2 process can be tested using Bio-In, H2-F, and SA-coupled magnetic beads (MBs) (Figure 2D): the first trigger caused by Bio-In further led to the formation of MCR assemblies with biotin tails, which could bind to MBs and be removed from the system via rapid magnetic

DOI: 10.1021/acsami.9b14452
ACS Appl. Mater. Interfaces 2019, 11, 36444–36448

separation.[34−36] The amount of removed H2-F reflected the degree of TSD2, which could be verified by weaker I_F of the collected supernatant compared to its control group (Figure 2E).

The size and morphology of MCR assemblies can be characterized by atomic force microscopy (AFM). As shown in Figure 3A, the AFM images indicate that MCR assemblies

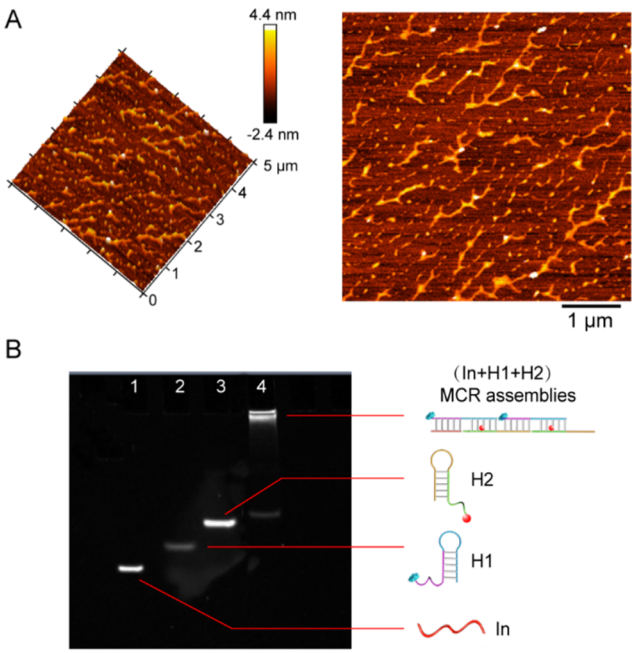

Figure 3. Characterization of the morphology and size of MCR assemblies by AFM and native PAGE. (A) Formed MCR assemblies measured by AFM. These linear assemblies are uniformly distributed on the surface. Some "branch" structures are observed in this figure, which might be generated due to uneven depositions of MCR assemblies during AFM sample preparation. (B) Native PAGE (15%) analysis of the formation of MCR assemblies. Lane 1: 2 μM In; Lane 2: 2 μM H1; Lane 3: 2 μM H2-F; and Lane 4: 0.1 μM In, 2 μM H1, and 2 μM H2-F.

maintained linear structures on the surface. The length and height of the formed linear assembly is around 1 μm and 2 nm, respectively. Although some assemblies are physically stacked due to sampling preparation, it can be clearly observed that the formed assemblies exhibited a uniform height along each linear MCR product. No linear products can be observed in the control group (Figure S1B), suggesting that the formation of MCR assemblies are triggered by In. The formation of MCR products can also be demonstrated by native polyacrylamide gel electrophoresis (PAGE). As shown in Figure 3B, the formed MCR assemblies in lane 4 exhibit a much lower migration speed than other short strands.

Next, the performances of DTB surface in managing the balance of MCR assembly capture and surface regeneration are investigated. Specifically, bovine serum albumin (BSA)−DTB conjugates with different molar ratios (0−75×) were synthesized, and the optimal conjugate to be further used was determined to be 50× BSA−DTB by comparing their sensitivities toward Cy5.5-labeled SA (SA-F) (Figures S2−S4). The grown SA layer was robust enough to resist buffer elution (Figure S5), which was applied in each of the following detections before MCR assembly injection to ensure minimal interferences from unbound SA-F. The rapid signal decrease observed in Figure S5 also indicated that the surface regeneration could be efficiently achieved using dilute acid (0.5% sodium dodecyl sulfate, pH 1.9). Under optimal conditions, different amounts of SA-F led to sensitive responses (Figure 4A), and its saturation concentration (20

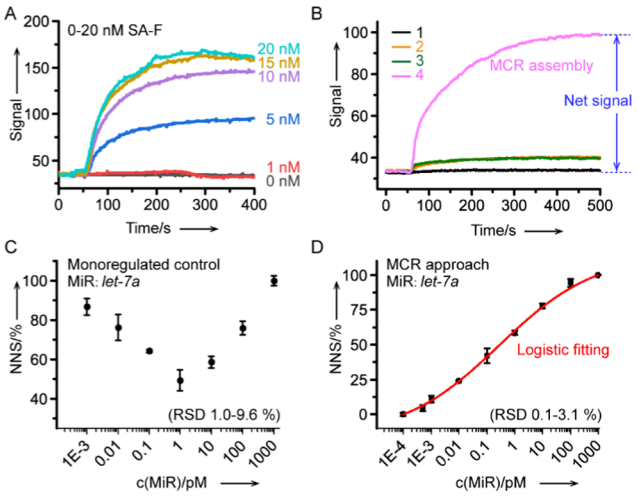

Figure 4. (A) Sensorgrams of 0−20 nM SA-F. (B) Specific signal response induced by biotinylated MCR assembly. Curve 1: 5 nM In + 50 nM Bio-H1; Curve 2: 5 nM In + 50 nM H2-F; Curve 3: 50 nM Bio-H1 + 50 nM H2-F (without In); and Curve 4: 5 nM In + 50 nM Bio-H1 + 50 nM H2-F. MiR calibration curves based on (C) monotag-regulated approach (control group) and (D) MCR approach. NNS = normalized net signal (signals generated by 0 and 1 nM of *let-7a* were set as 0 and 100%, respectively). Original sensorgrams corresponding to (C) and (D) are shown in Figures S6 and S7, respectively.

nM) was applied to guarantee sufficient SA coverage. Furthermore, the specificity of the designed surface was evaluated (Figure 4B): neither Bio-H1 nor H2-F showed obvious signals after being incubated with In. Besides, the cascade leakage caused by spontaneous hybridization between two hairpins was also minor, as demonstrated by low signals generated by co-incubated Bio-H1 and H2-F. In contrast, MCR assembly led to an approximate 10×-fold signal increase, which is satisfactory among developed nucleic acid based fluorescent biosensors.[37]

Given the specific high FL enhancement toward biotinylated products, the sensing performances using MCR and its control group were compared. As expected, the monotag-regulated control exhibited diverse signaling distances, making it unqualified for miR sensing due to non-monotonic responses (Figure 4C). We speculate that the observed V-shaped curve in Figure 4C is caused by the differences in the assembling efficiencies triggered by different amounts of miR. However, the MCR assay operated reliably with smaller signal deviations in the presence of 0.1 fM to 1 nM of *let-7a* (Figure 4D). Normalized net signals (NNS) in Figure 4D are fitted by the four-parameter Logistic model, and the LOD toward miR is calculated to be 0.8 fM with a linear range from 1 fM to 71 pM (5 orders of magnitude) (Page S-5, Section 7). This sensitivity is around 30 000-fold higher than that of the MCR-free system using the same optical-fiber biosensor (LOD 24 pM)[25] and is comparable to that of other reported miR biosensing approaches (Table S3). Besides, the signals obtained by this MCR approach are selective toward target miR (*let-7a*) (Figure

DOI: 10.1021/acsami.9b14452
ACS Appl. Mater. Interfaces 2019, 11, 36444−36448

S8). Moreover, the applicability of this MCR approach has also been verified using human urine samples. As shown in Figure S9, the MCR signals gradually increased in the presence of 0.1 fM to 1 nM of *let-7a*. After the four-parameter Logistic model fitting of signals in Figure S9, the LOD toward miR in the urine sample using this MCR method is calculated to be 0.1 fM, exhibiting a slightly higher sensitivity than that in the buffer condition.

Taking advantage of the prominent miR sensing features of MCR using signaling-distance-sensitive biosensors, we further operated MCR in clinical samples. Urine samples of patients with nonsmall cell lung cancer (NSCLC) or unspecified lung cancer (USLC) were donated by two hospitals in Beijing. Other urine samples were collected from voluntary healthy donors. Using our MCR approach, reduced expression levels of *let-7a* in the NSCLC group and USLC were distinctly observed (Figure 5A), which was in accordance with the previous

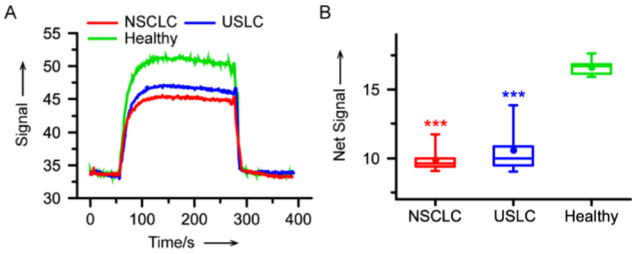

Figure 5. (A) Representative urinary miR detection sensorgrams. (B) Distinguishing cancer patients (NSCLC and USLC) from healthy donors through net MCR signals generated by urinary miR (N = 9, p = 0.001).

research.[38] Besides, the extremely significant difference between net signals of three groups (Figure 5B) demonstrated the feasibility of MCR approach in cancer prognosis. Moreover, the MCR approach also features inexpensive enzyme-free system and a reusable DTB surface that allows over 100 successive cycles (Figure S10).

CONCLUSIONS

In sum, we have rationally designed a multitag-regulated cascade reaction (MCR) as a general amplification approach for trace miR detection. For the first time, the surface regulation of complex nucleic acid assemblies by multitag approach is realized. Based on a signaling-distance-sensitive optical-fiber biosensor, a 30 000-fold improved sensitivity (LOD 0.8 fM) is achieved compared with the MCR-free method. Moreover, the MCR approach exhibits a large dynamic range of 5 orders of magnitude and a demonstrated cancer prognosis capacity. Overall, our work highlights the important and practical role of MCR in developing ultrasensitive miR biosensors for cancer prognosis, which can be easily generalized to the regulation of other functional nucleic acid assemblies and opens a broad field for enzyme-free biosensing applications.

ASSOCIATED CONTENT

Supporting Information

The Supporting Information is available free of charge on the ACS Publications website at DOI: 10.1021/acsami.9b14452.

Materials, instruments, and experimental procedures; and experimental results and discussion, including protein recovery rates of different BSA-DTB conjugates; sensing performance of other miR assays/biosensors; schematic illustration of the monotag-regulated approach and AFM characterization, synthesis reaction of BSA-DTB, and preparation of DTB functionalized optical-fiber; net signals of optical fibers modified with different types of BSA−DTB conjugates; sensorgram during one test cycle; origianl sensorgrams corresponding to Figure 4C and 4D; selectivity of the developed MCR approach; normalized net signals (NNS) against different miR concentrations in urine samples; and NNS against one sample in different regeneration cycles (PDF)

AUTHOR INFORMATION

Corresponding Author

*E-mail: xhzhou@mail.tsinghua.edu.cn. Tel: (010) 6279-6953.

ORCID

Ruoyu Wang: 0000-0002-7091-0291

Xiaohong Zhou: 0000-0002-5307-6709

Notes

The authors declare no competing financial interest.

ACKNOWLEDGMENTS

We thank Associate Professor Dr. Yu Xiang from the Department of Chemistry, Tsinghua University for helpful discussion and valuable research advice. The authors acknowledge the Beijing Aizhen Hospital and Beijing Cancer Hospital for assistance with cancer patient urine collection. This work was supported by National Nature Science Foundation of China (21677082).

REFERENCES

(1) Chanock, S. J. The Paradox of Mutations and Cancer. *Science* **2018**, *362*, 893−894.

(2) Luo, D.; Carter, K. A.; Miranda, D.; Lovell, J. F. Chemophototherapy: An Emerging Treatment Option for Solid Tumors. *Adv. Sci.* **2017**, *4*, No. 1600106.

(3) Drusco, A.; Croce, C. M. MicroRNAs and Cancer: A Long Story for Short RNAs. *Adv. Cancer Res.* **2017**, *135*, 1−24.

(4) Masud, M. K.; Umer, M.; Hossain, M. S. A.; Yamauchi, Y.; Nguyen, N. T.; Shiddiky, M. J. A. Nanoarchitecture Frameworks for Electrochemical miRNA Detection. *Trends Biochem. Sci.* **2019**, *44*, 433−542.

(5) Miao, P.; Tang, Y.; Wang, B.; Meng, F. Near-Infrared Ag_2S Quantum Dots-Based DNA Logic Gate Platform for miRNA Diagnostics. *Anal. Chem.* **2016**, *88*, 7567−7573.

(6) Kozomara, A.; Griffiths-Jones, S. Mirbase: Annotating High Confidence MicroRNAs Using Deep Sequencing Data. *Nucleic Acids Res.* **2014**, *42*, D68−D73.

(7) Kilic, T.; Erdem, A.; Ozsoz, M.; Carrara, S. MicroRNA Biosensors: Opportunities and Challenges among Conventional and Commercially Available Techniques. *Biosens. Bioelectron.* **2018**, *99*, 525−546.

(8) Johnson, B. N.; Mutharasan, R. Biosensor-Based MicroRNA Detection: Techniques, Design, Performance, and Challenges. *Analyst* **2014**, *139*, 1576−1588.

(9) Zhai, Q.; He, Y.; Li, X.; Guo, J.; Li, S.; Yi, G. A Simple and Ultrasensitive Electrochemical Biosensor for Detection of MicroRNA Based on Hybridization Chain Reaction Amplification. *J. Electroanal. Chem.* **2015**, *758*, 20−25.

(10) Islam, M. N.; Masud, M. K.; Haque, M. H.; Hossain, M. S. A.; Yamauchi, Y.; Nguyen, N. T.; Shiddiky, M. J. RNA Biomarkers:

DOI: 10.1021/acsami.9b14452
ACS Appl. Mater. Interfaces 2019, 11, 36444−36448

Diagnostic and Prognostic Potentials and Recent Developments of Electrochemical Biosensors. *Small Methods* **2017**, *1*, No. 1700131.
(11) Islam, M. N.; Masud, M. K.; Nguyen, N. T.; Gopalan, V.; Alamri, H. R.; Alothman, Z. A.; Hossain, M. S. A.; Yamauchi, Y.; Lam, A. K.; Shiddiky, M. J. A. Gold-Loaded Nanoporous Ferric Oxide Nanocubes for Electrocatalytic Detection of MicroRNA at Attomolar Level. *Biosens. Bioelectron.* **2018**, *101*, 275−281.
(12) Kamal Masud, M.; Islam, M. N.; Haque, M. H.; Tanaka, S.; Gopalan, V.; Alici, G.; Nguyen, N. T.; Lam, A. K.; Hossain, M. S. A.; Yamauchi, Y.; Shiddiky, M. J. A. Gold-Loaded Nanoporous Superparamagnetic Nanocubes for Catalytic Signal Amplification in Detecting MiRNA. *Chem. Commun.* **2017**, *53*, 8231−8234.
(13) Zhang, D. Y.; Seelig, G. Dynamic DNA Nanotechnology Using Strand-Displacement Reactions. *Nat. Chem.* **2011**, *3*, 103−113.
(14) Chirieleison, S. M.; Allen, P. B.; Simpson, Z. B.; Ellington, A. D.; Chen, X. Pattern Transformation with DNA Circuits. *Nat. Chem.* **2013**, *5*, 1000−1005.
(15) Yao, G.; Li, J.; Chao, J.; Pei, H.; Liu, H.; Zhao, Y.; Shi, J.; Huang, Q.; Wang, L.; Huang, W.; Fan, C. Gold-Nanoparticle-Mediated Jigsaw-Puzzle-Like Assembly of Supersized Plasmonic DNA Origami. *Angew. Chem.* **2015**, *127*, 3009−3012.
(16) Dirks, R. M.; Pierce, N. A. Triggered Amplification by Hybridization Chain Reaction. *Proc. Natl. Acad. Sci. U.S.A.* **2004**, *101*, 15275−15278.
(17) Bi, S.; Yue, S.; Zhang, S. Hybridization Chain Reaction: A Versatile Molecular Tool for Biosensing, Bioimaging, and Biomedicine. *Chem. Soc. Rev.* **2017**, *46*, 4281−4298.
(18) Wen, Y.; Liu, G.; Pei, H.; Li, L.; Xu, Q.; Liang, W.; Li, Y.; Xu, L.; Ren, S.; Fan, C. DNA Nanostructure-Based Ultrasensitive Electrochemical MicroRNA Biosensor. *Methods* **2013**, *64*, 276−282.
(19) Zhu, D.; Liu, W.; Cao, W.; Chao, J.; Su, S.; Wang, L.; Fan, C. Multiple Amplified Electrochemical Detection of MicroRNA-21 Using Hierarchical Flower-Like Gold Nanostructures Combined with Gold-Enriched Hybridization Chain Reaction. *Electroanalysis* **2018**, *30*, 1349−1356.
(20) Li, M.; Lv, M.; Wang, L.; Fan, C.; Zuo, X. Engineering Electrochemical Interface for Biomolecular Sensing. *Curr. Opin. Electrochem.* **2019**, *14*, 71−80.
(21) Cao, S. H.; Xie, T. T.; Cai, W. P.; Liu, Q.; Li, Y. Q. Electric Field Assisted Surface Plasmon-Coupled Directional Emission: An Active Strategy on Enhancing Sensitivity for DNA Sensing and Efficient Discrimination of Single Base Mutation. *J. Am. Chem. Soc.* **2011**, *133*, 1787−1789.
(22) Ronkainen, N. J.; Halsall, H. B.; Heineman, W. R. Electrochemical Biosensors. *Chem. Soc. Rev.* **2010**, *39*, 1747−1763.
(23) Gauglitz, G. Direct Optical Sensors: Principles and Selected Applications. *Anal. Bioanal. Chem.* **2005**, *381*, 141−155.
(24) Wang, R. Y.; Zhou, X. H.; Zhu, X. Y.; Yang, C.; Liu, L. H.; Shi, H. C. Isoelectric Bovine Serum Albumin: Robust Blocking Agent for Enhanced Performance in Optical-Fiber Based DNA Sensing. *ACS Sens.* **2017**, *2*, 257−262.
(25) Zhu, X. Y.; Wang, R. Y.; Zhou, X. H.; Shi, H. C. Free-Energy-Driven Lock/Open Assembly-Based Optical DNA Sensor for Cancer-Related MicroRNA Detection with a Shortened Time-to-Result. *ACS Appl. Mater. Interfaces* **2017**, *9*, 25789−25795.
(26) Taitt, C. R.; Anderson, G. P.; Ligler, F. S. Evanescent Wave Fluorescence Biosensors: Advances of the Last Decade. *Biosens. Bioelectron.* **2016**, *76*, 103−112.
(27) Ge, Z.; Lin, M.; Wang, P.; Pei, H.; Yan, J.; Shi, J.; Huang, Q.; He, D.; Fan, C.; Zuo, X. Hybridization Chain Reaction Amplification of MicroRNA Detection with a Tetrahedral DNA Nanostructure-Based Electrochemical Biosensor. *Anal. Chem.* **2014**, *86*, 2124−2130.
(28) Yang, L.; Liu, C.; Ren, W.; Li, Z. Graphene Surface-Anchored Fluorescence Sensor for Sensitive Detection of MicroRNA Coupled with Enzyme-Free Signal Amplification of Hybridization Chain Reaction. *ACS Appl. Mater. Interfaces* **2012**, *4*, 6450−6453.
(29) Zhu, Q.; Chai, Y.; Zhuo, Y.; Yuan, R. Ultrasensitive Simultaneous Detection of Four Biomarkers Based on Hybridization Chain Reaction and Biotin−Streptavidin Signal Amplification Strategy. *Biosens. Bioelectron.* **2015**, *68*, 42−48.
(30) Guo, Q.; Bian, F.; Liu, Y.; Qu, X.; Hu, X.; Sun, Q. Hybridization Chain Reactions on Silica Coated Qbeads for the Colorimetric Detection of Multiplex MicroRNAs. *Chem. Commun.* **2017**, *53*, 4954−4957.
(31) Xuan, F.; Hsing, I. M. Triggering Hairpin-Free Chain-Branching Growth of Fluorescent DNA Dendrimers for Nonlinear Hybridization Chain Reaction. *J. Am. Chem. Soc.* **2014**, *136*, 9810−9813.
(32) Ang, Y. S.; Yung, L. L. Rational Design of Hybridization Chain Reaction Monomers for Robust Signal Amplification. *Chem. Commun.* **2016**, *52*, 4219−4222.
(33) Wolfe, B. R.; Porubsky, N. J.; Zadeh, J. N.; Dirks, R. M.; Pierce, N. A. Constrained Multistate Sequence Design for Nucleic Acid Reaction Pathway Engineering. *J. Am. Chem. Soc.* **2017**, *139*, 3134−3144.
(34) Zhou, Z.; Xiang, Y.; Tong, A.; Lu, Y. Simple and Efficient Method to Purify DNA−Protein Conjugates and Its Sensing Applications. *Anal. Chem.* **2014**, *86*, 3869−3875.
(35) Wang, R. Y.; Xiang, Y.; Zhou, X. H.; Liu, L. H.; Shi, H. C. , A Reusable Aptamer-Based Evanescent Wave All-Fiber Biosensor for Highly Sensitive Detection of Ochratoxin A. *Biosens. Bioelectron.* **2015**, *66*, 11−18.
(36) Wang, R. Y.; Zhou, X. H.; Shi, H. C. Triple Functional DNA−Protein Conjugates: Signal Probes for Pb^{2+} Using Evanescent Wave-Induced Emission. *Biosens. Bioelectron.* **2015**, *74*, 78−84.
(37) Chiuman, W.; Li, Y. Efficient Signaling Platforms Built from a Small Catalytic DNA and Doubly Labeled Fluorogenic Substrates. *Nucleic Acids Res.* **2007**, *35*, 401−405.
(38) Takamizawa, J.; Konishi, H.; Yanagisawa, K.; Tomida, S.; Osada, H.; Endoh, H.; Harano, T.; Yatabe, Y.; Nagino, M.; Nimura, Y.; Mitsudomi, T.; Takahashi, T. Reduced Expression of the Let-7 MicroRNAs in Human Lung Cancers in Association with Shortened Postoperative Survival. *Cancer Res.* **2004**, *64*, 3753−3756.

DOI: 10.1021/acsami.9b14452
ACS Appl. Mater. Interfaces 2019, 11, 36444−36448